論文

인발-와인딩에 의한 불포화수지 섬유강화 중공봉의 기계적 거동해석

김조권*, 린 예**

Analysis of Mechanical Behavior for a Pultruded-Wound Hollow Rod of Unsaturated Polyester Resin(UP) with Glass Fibers

Zoh-Gweon Kim* , Lin Ye**

ABSTRACT

Analysis of mechanical behavior for a pultruded-wound hollow rod is presented. For this purpose, the pultruded-wound hollow rod is manufactured by the new winder attached to the conventional pultrusion system. And the conventional pultrusion process is newly altered to manufacture pultruded-wound specimens. A computer program, POSTⅡ, is modified to perform this study. In the nonlinear finite element formulation, the updated Lagrangian description method based on the second Piolar-Kirchhoff stress tensor and the Green strain tensor are used. For the finite element modeling of the composite hollow rod, the eight-node degenerated shell element is utilized. In order to estimate the failure, the maximum stress criterion is adopted to the averaged stress in the each layer of the finite elements. As numerical examples, the behavior of glass/UP composite hollow rod is investigated from the initial loading to the final collapse. Present finite element results considering stiffness degradation and stress unload due to failure shows excellent agreement with experiments in the ultimate load, failure and deformations.

초 록

인발 와인딩에 의한 섬유강화 복합재료 중공 봉의 기계적 거동해석을 수행하였다. 이 목적의 수행을 위해 새롭게 제작된 와인더를 전통적 인발 시스템에 부착하여 시편을 제작하였다. 또한 인발-와인딩된 시편을 제작할 수 있는 새로운 공법을 개발하였다. 이 연구를 위해 유한요소 해석 프로그램 POSTⅡ를 확장 개발하였다. 비선형유한요소 수식화에는 2차 피올라-키르히호프 응력 텐서와 그린 변형률 텐서에 기초한 업데이트된 라그란지언 표현법이 사용되었다. 복합재료 중공 봉의 유한요소 모델링을 위해 8절점 응축쉘요소를 사용하였다. 파손평가를 위해 모든 유한요소의 각 단층에서의 평균응력을 최대응력 판정법에 대입하였다. 수치해석 예로서 불포화 섬유강화 복합재료 중공 봉의 기계적 거동을 초기 하중상태에서 최종 붕괴까지 조사하였다. 파손에 따른 강성저하와 응력제하를 고려한 유한요소해석 결과는 극한 하중과 파손 및 변형에서 실험치와 잘 일치하였다.

1. Introduction

Application of fiber reinforced composite materials in most industries has caused interest in accurate prediction of the characteristics of composite structures. In order to predict the accurate behavior of composite structures, the entire non-linear behavior must be analyzed. Recently, extensive research on the pultrusion is reported in the open literatures.

* 창원기능대학, 교신저자(E-mail:zokim@cw-polytec.ac.kr)
** 시드니대학교 기계자동화공학부

Much of the work are confined to the unidirectional composites and such a process has been taken for grated. Price[1] analyzed first the thermortheological aspects of the processing of epoxy-carbon fiber and polyester-glass fiber. Sumerak[2] conducted the experiment on the pulling force, the temperature and the resin pressure distribution inside the die. Raper et al[3] developed a mathematical model based on Darcy's law to obtain the pressure and velocity fields in a pultrusion die. Batch[4] performed numerical calculation for temperature and pulling force as well as experiments measuring temperature distribution. Sharma[5] developed a more complete analysis of the pressure rise in the tapered inlet region of the pultrusion die and employed the finite element method to predict the pressure as a function of various process control parameters. Moschiar et al[6] performed an analysis of the pultrusion processing for thermosetting matrix composites. The development of pressure in the die and the required pulling force are modeled and compared with experimental results. Kim[7] performed the entire postbuckling behavior of stiffened composite laminated cylindrical panels using the finite element method based on the updated Lagrangian formulation. In this study, mechanical behavior of pultruded-wound hollow rod of unasturated polyester resin with glass fiber are analyzed and compared with the experimental data. For experiments, various pultruded-wound hollow rods are manufactured by the new winder attached to the conventional pultrusion system. Also, the analytic principle of the program is presented.

2. Nonlinear Finite Element Analysis

The present study utilizes the formulation of geometrically nonlinear finite element procedures based on the updated Lagrangian description with the second Piola-Kirchhoff stress and Green Lagrangian strain, and the eight node degenerated shell element for finite element modeling of the pultreded-wound rod structure. The updated Lagrangian formulation describes equilibrium at a particular load step by dint of a previously known equilibrium configuration. If equilibrium is obtained at a certain load level, state variables are updated for the initial values of the next configuration.

2.1 Formulation of the finite element equation

In order to model a shell element, the degenerated three dimensional isoparametric solid element with independent rotational and translational degrees of freedom is utilized. Applying this element for the finite element formulation, two basic assumptions: lines originally normal to the shell mid-surface remains straight and transverse normal stresses remain zero are employed in the shell theory. The details of the finite element formulation by the degenerated shell element can be referred to reference[8]. The final incremental equation for an element is depicted by

$$([K_L] + [K_{NL}]) \{\Delta U\} = -\{\Delta P\} \quad (1)$$

where $[K_L]$ is the linear element stiffness matrix, $[K_{NL}]$ is the nonlinear element stiffness matrix, $\{\Delta U\}$ is the vector of nodal degrees of freedom, and $\{\Delta P\}$ is the incremental load. Incremental displacement fields in an element are depicted as

$$\begin{Bmatrix} \Delta u \\ \Delta v \\ \Delta w \end{Bmatrix} = \sum_{n=1}^{8} H_n(\xi,\eta) \begin{Bmatrix} \Delta u_n \\ \Delta v_n \\ \Delta w_n \end{Bmatrix} + \frac{1}{2} \sum_{n=1}^{8} H_n t_n \zeta \{\Delta V_{n\zeta}\} \quad (2)$$

where ζ, η and ξ are local coordinates in the element. H_n, t_n and $\{\Delta V_{n\zeta}\}$ are shape function, thickness and increment of the vector in ζ -direction at nth node, respectively. The nodal displacements and rotation can be computed by assembling element stiffness matrix and force vectors and by solving the incremental finite element equation at each incremental load step. Then corresponding state variables can be obtained from nodal displacements and rotations. Since the incremental second Piola-Kirchhoff stress has little physical meaning definitely, it should be converted to the incremental Cauchy stress which provides the initial stress of the next incremental load step as follows

$$\sigma_{ij} = \frac{1}{det[F]} F_{ik} F_{jl} (\sigma_{ij} + \Delta S_{ij}) \quad (3)$$

where σ_{kl} is the Cauchy stress, ΔS_{kl} is the incremental second Piolar-Kirchoff stress, and [F] is the deformation gradient found in reference[8].

2.2 Failure Model

The average stress in each direction of a layer is substituted

into the maximum stress criterion and failure of each layer is identified. The maximum stress criteria used in this failure analysis are

$$\sigma_1^m > X_T \qquad \sigma_1^m < X_C$$
$$\sigma_2^m > Y_T \qquad \sigma_2^m < Y_C \qquad (4)$$
$$\tau_{12}^m > S \qquad \tau_{12}^m < -S$$

where, X, Y and S are the strength in 1-axis direction, in 2-axis direction, and shear strength in 1-2 plane, respectively. Subscripts 1 and 2 mean the fiber direction and the transverse direction, and T and C stand for tension and compression. If failure occurs and progresses, the stiffness of the structure and the load to be carried remove. Complete unloading model is utilized in this approach. This model is the most conventional failure model, which can remove the stiffness and the stress of failed layer completely.

3. Description of the problem

In this study, various pultruded-wound hollow rod is analyzed. The axial fibers are indicated as $\theta=0°$ and the wound fibers are oriented in $\theta=\pm\alpha°$ as shown in Fig.1. Models to be analyzed is shown in Table 2 by various winding sequences. Engineering constants of glass/UP(made by KCC Co.) for the present analysis are in Table 1. The geometry and the dimensions of the hollow rod are also shown in Fig.1 and the dimensions are L=700mm, out diameter=11.5mm, and inner diameter=4.5mm.

Table 1 Material Properties of KCC glass/UP composites matrrials

Property	Symbol	Value
Elastic modulus in for fiber direction	E_1	21.5 GPa
Elastic modulus in transverse direction	E_2 E_3	2.7 GPa
Shear moduli in 1-2, 1-3 and 2-3 planes	G_{12} $G_{13}G_{23}$	2.4 GPa
Major poisson's ration	ν_{12}	0.28
Tensile strength in fiber-direction	X_T	620 MPa
Compressive strength in fiber-direction	X_C	359 MPa
Tensile strength in transverse diction	Y_T	39.1 MPa
Compressive strength in transverse diction	Y_C	148 MPa
shear strength	S	102.9 MPa

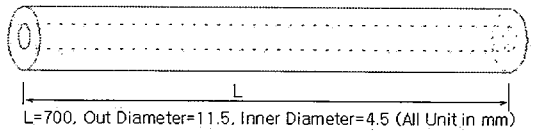

Fig. 1 Geometry of typical specimen.

Table 2 Buckling load and postbuckling ultimate load for various pultruded-wound hollow rods

Model	Winding sequence	Tension		Bending	
		$P_{CR}(N)$	$P_{UL}(N)$	$P_{CR}(N)$	$P_{UL}(N)$
TA(BA)	$[O_8]_T$		40067.78	4709.02	8929.53
TB(BB)	$[90_2/O_6]_T$	8112.45	32345.25	4700.04	8412.34
TC(BC)	$[O_2/90_2/O_4]_T$	8018.67	30945.76	4557.04	7589.62
TD(BD)	$[O_2/90_2/O_2]_T$	7414.00	29762.13	4713.04	8143.24
TE(BE)	$[O_6/90_2]_T$	7127.01	28313.02	4631.43	7633.79
TF(BF)	$[45_2/O_6]_T$	8200.13	34001.77	5964.44	8396.71
TG(BG)	$[60_2/O_6]_T$		32101.48	6829.49	8106.25
TH(BH)	$[30_2/O_6]_T$		32128.64	6001.68	7914.24
TY(BY)	$[O_3/\pm45/O_3]_T$		33915.14	6008.41	8283.29
TX(BX)	$[O/\pm45/O_5]_T$		37586.23	4253.32	10723.43
TW(BW)	$[O_2/\pm45/O_4]_T$		41403.88	4953.90	9648.38
TZ(BZ)	$[O_2/\pm45/O_2]_T$		31473.99	7809.70	9515.00

4. Experiment

The specimens are manufactured by the system as shown in Fig. 2. In this case, the devised winder is attached to the conventional pultrusion system to give the various wound angles. The winder has a resin bath which has the special squeeze bushings and appropriate guide apparatus for wetting and forming the wound angle. The curing temperature is controlled at 80℃ in the first heated forming die and at 220℃ in the second heater. The pulling speed is controlled 600mm/min and the winder has the variable rotating speed to give various wound angle. The tension and bending tests were conducted to verify the finite element analysis of the pultruded-wound hollow rod. Tensile test was performed in accordance with ASTM D3916-94 & D 2105-90 specifications, and three-point bending test was performed

according to ASTM D 4476-85. In the tensile test, mild steel tabs contoured to the shape of the hollow rod are used to reduce the high transverse-compressive forces imparted to the rod, thus overcoming the premature failure influenced by the conventional method of gripping. In the bending test, the loading nose with cylindrical surfaces is used in order to avoid excessive indentation or failure due to stress concentration directly under the loading nose. The radious of the nose is 10mm for all specimen. The rod was loaded by uniform displacement at both ends in tension, and at mid in bending. The rod specimen was tested to failure so as to determine the postbuckling behavior in static tension and bending. A LVDT was used to measure the displacement for tension and bending. As shown in Fig. 3 and 4, the bending results of the finite element analysis is well consistent with the experiment with difference of 0.2% in buckling load and 0.1% in postbuckling ultimate load. Tension result is excellently consistent without difference in the postbuckling ultimate load. The small difference between experiment and analysis at equilibrium path may be due to the initial slip, misalignment and imperfect boundary condition.

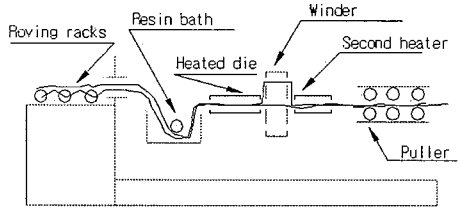

Fig. 2 Schematic diagram of pultruded-wound system.

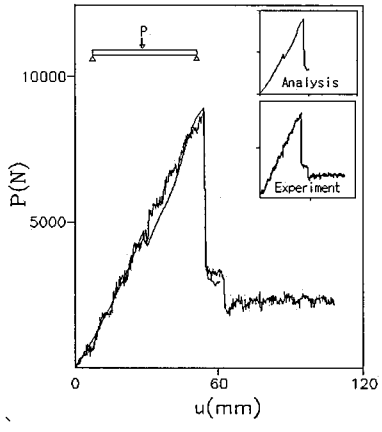

Fig. 3 Load-deflection curves for hollow rod under bending.

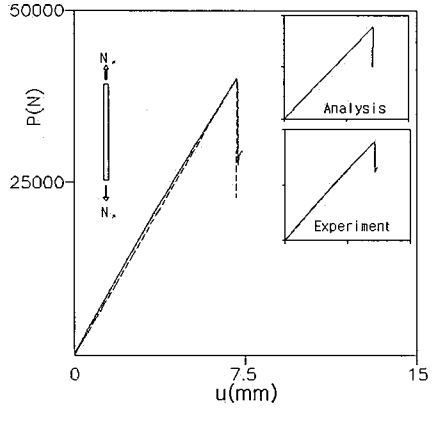

Fig. 4 Load-extension curves for hollow rod under tension.

5. Results and Discussion

5.1 Buckling behavior in tension

Table 2 shows the effect of winding angle and winding location on the buckling load and the postbuckling ultimate

Table 3 Normalized extensional stiffness for several rod elements

Model	Normalized extensional stiffness(GPa), A*					
	A_{11}	A_{12}	A_{22}	A_{16}	A_{26}	A_{66}
TA(BA)	21.75	0.82	0.00	2.73	0.00	2.70
TB(BB)	16.99	0.82	0.00	7.48	0.00	2.70
TC(BC)	16.99	0.82	0.00	7.48	0.00	2.70
TD(BD)	16.99	0.82	0.00	7.48	0.00	2.70
TE(BE)	16.99	0.82	0.00	7.48	0.00	2.70
TF(BF)	18.62	1.57	1.19	4.36	1.19	3.45
TG(BG)	17.62	1.38	0.70	5.73	1.36	3.26
TH(BH)	19.99	1.38	1.36	3.36	0.70	3.26
TY(BY)	18.62	1.57	0.00	4.36	0.00	3.45
TZ(BZ)	18.62	1.57	0.00	4.36	0.00	3.45
TW(BW)	18.62	1.57	0.00	4.36	0.00	3.45
TX(BX)	18.62	1.57	0.00	4.36	0.00	3.45

$A^* = A/t$

load. Figure 5 indicates the effects of winding location on the winding angle with 90°, and shows that TB, TC, TD and TE were buckled. Table 3 shows that the smaller A_{11}, A_{12} and the larger A_{16} influence the buckling of TB,TC,TD, and TE. Figure 6 shows the effects of various winding angle in the outer layer of the rod, and shows that TB and TF were buckled. Figure 7 shows the effects of winding angle with ± 45° in the mid-layer of the rod, and shows that any models are not buckled. Table 3 shows that all values of A are equal. This is because of the intrinsic characteristics of composite material governed not by only one stiffness component of the extensional stiffness matrix but coupling action of various stiffness matrix.

5.2 Buckling behavior in bending

Figure 8 shows the effects of winding location on the winding angle with 90°. Figure 9 shows the effects of various winding angle in the outer layer of the rod and Figure 10 shows the effects of winding angle with ±45° in the mid-layer of the rod. All models were buckled once at least. Figure 8 indicates that BA has the larger buckling load and the larger bending stiffness D_{11}. However, comparing only D_{11} in table 5, the D_{11} of BA is 0.5% larger than the D_{11} of BC but the postbuckling ultimate load of BA is 29% larger than BC. Hence it is thought to be affected not only by bending stiffness matrix but by coupling action of various stiffness matrix to increase the postbuckling ultimate load. BX has the larger buckling load from Table 2 and Fig. 9. It shows a rise of 45% over BA. In order to increase the buckling load, it is necessary to choose the reasonable winding angle and the winding location.

Table 4 Normalized coupling stiffness for several rod elements

Model	Normalized coupling stiffness(GPa), B*					
	B_{11}	B_{12}	B_{22}	B_{16}	B_{26}	B_{66}
TA(BA)	0.00	0.00	0.00	0.00	0.00	0.00
TB(BB)	3.57	0.00	0.00	-0.37	0.00	0.00
TC(BC)	1.19	0.00	0.00	-1.19	0.00	0.00
TD(BD)	-1.19	0.00	0.00	1.19	0.00	0.00
TE(BE)	-3.57	0.00	0.00	3.57	0.00	0.00
TF(BF)	2.35	-0.56	-0.89	-1.22	-0.89	-0.56
TG(BG)	3.10	-0.42	-0.53	-2.25	-1.02	-0.42
TH(BH)	1.31	-0.42	-1.02	-0.47	-0.53	-0.42
TY(BY)	0.00	0.00	-0.15	0.00	-0.15	0.00
TZ(BZ)	-0.78	0.19	-0.15	0.41	-0.15	0.19
TW(BW)	0.78	-0.19	-0.15	-0.41	-0.15	-0.19
TX(BX)	1.56	-0.38	-0.15	-0.81	-0.15	-0.38

$B^* = 2B/t$

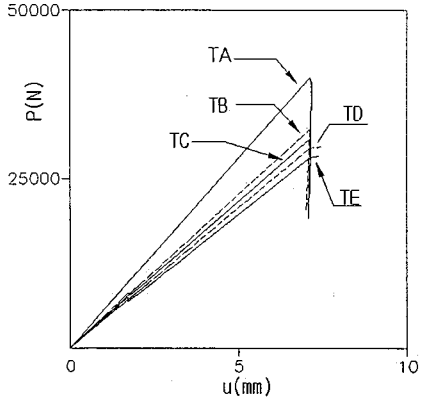

Fig. 5 Load-extension curves for models wound at 90°.

5.3 Postbuckling behavior in tension

Figure 5 shows that the load carrying capacity of buckled models increases linearly to the failure after buckling. TA has the largest ultimate load and A_{11}, but it is confirmed from Table 3 that the largest ultimate load is affected by extensional stiffness matrix and coupling action of several stiffness matrix. Figure 6 shows that the load carrying

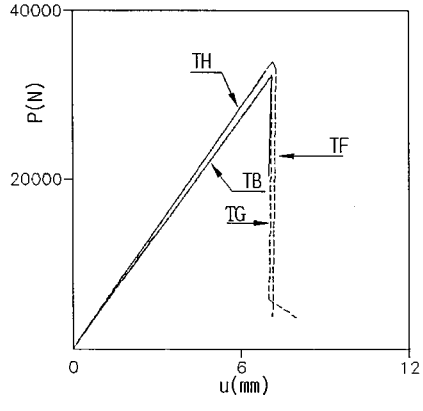

Fig. 6 Load-extension curves for models wound at various angles.

capacity of all models increases linearly to the failure without buckling and that all equilibrium path is affected by various angle of the outer layer. TG has the largest ultimate load but a decrease of 15% over TA. Figure 7 shows that all models has nearly no additional load carrying capacity after failure. TW has the largest ultimate load and a rise of 3.3% over TA. TW shows a rise of 3.3% in ultimate load and a rise of 29% in elongation over TA. The increase of ultimate load is also affected by extensional stiffness matrix and coupling action of various stiffness matrix.

5.4 Postbuckling behavior in bending

Figure 8 indicates that all models are buckled once at least and they have nearly no additional load carrying capacity after failure. BC shows that a burst deformation occurs after the second buckling. BA shows the larger postbuckling ultimate load and the larger D_{11}. But, Figure 8 and table 5 show that the larger postbuckling load is determined by bending stiffness matrix and by coupling action of several seiffness matrix. Figure 9 shows that most models are also buckled once at least, and that the angle variance of the outer layer affects the postbuckling ultimate load but that bending stiffness matrix does not affect it directly. Figure 10 shows that BX has the larger postbuckling load and some additional load carrying capacity after failure. All models of Figure 10 have the larger postbuckling load then BA except BY. The postbuckling load of BX is in a rise of 20% over BA. Hence the reasonable winding angle and winding location enables the postbuckling load to increase from Table 2 and 5.

Table 5 Normalized bending stiffness for several rod elements

Model	Normalized bending stiffness(GPa), D*					
	D_{11}	D_{12}	D_{22}	D_{16}	D_{26}	D_{66}
TA(BA)	21.75	0.82	0.00	2.73	0.00	2.70
TB(BB)	13.43	0.82	0.00	11.05	0.00	2.70
TC(BC)	20.56	0.82	0.00	3.92	0.00	2.70
TD(BD)	20.56	0.82	0.00	3.92	0.00	2.70
TE(BE)	13.43	0.82	0.00	11.05	0.00	2.70
TF(BF)	16.27	2.14	2.08	5.57	2.08	4.02
TG(BG)	14.52	1.81	1.23	7.98	2.37	3.69
TH(BH)	18.68	1.81	2.37	3.82	1.23	3.69
TY(BY)	21.55	0.87	0.00	2.83	0.00	2.75
TZ(BZ)	20.96	1.00	-0.22	3.14	-0.22	2.89
TW(BW)	20.96	1.00	0.22	3.14	0.22	2.89
TX(BX)	19.20	1.43	0.45	4.05	0.45	3.31

$D^* = 12D/t^3$

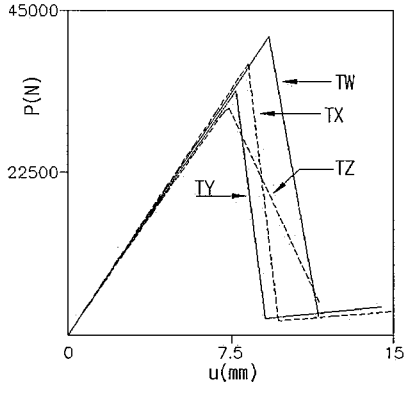

Fig. 7 Load-extension curves for models wound at ±45°.

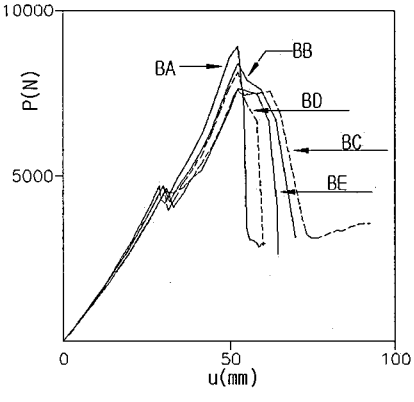

Fig. 8 Load-deflection curves for models wound at 90°.

5.5 Failure characteristics

Matrix failure mode, shear failure mode and fiber failure mode are considered in this study. The general faulure mode of no wound tension specimen shows that many tension fiber failure occur first at the mid-rod when the load reaches near the ultimate load. Then, many fibers failure and matrix failure propagates over the entire rod immediately after the

ultimate load. The failure appearance of model TA is shown in Fig. 11. The general faulure appearance of wound tension apecimen shows that the tension matrix fail occurs continuously right before the ultimate load, and tension fiber fail appears in large quantities just over the ultimate load. The failure appearance of model TE is shown in Fig. 12.

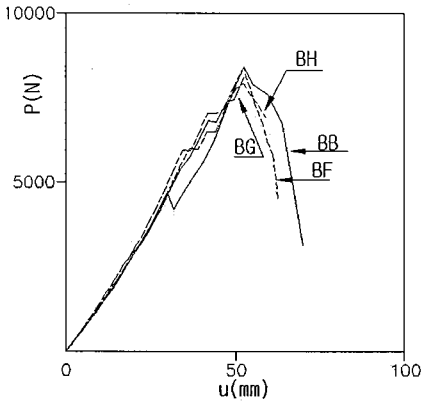

Fig. 9 Load-deflection curves for models wound at various angle.

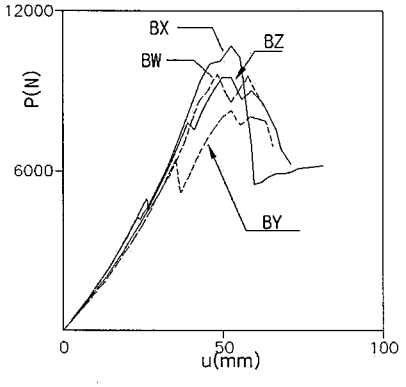

Fig. 10 Load- deflection curves for models wound at ±45°.

The general failure appearance of no wound bending specimen shows that shear matrix fail occurs continuously from near the first buckling to the second buckling. Then, tension fiber failure mode appears when the load reaches over the ultimate load. The failure appearance of model BA is shown in Fig. 13. The general failure mode of wound bending specimens shows that tension matrix fail occurs first near the first buckling, and shear matrix failure mode appears continuously over the first buckling. Then, tension matrix fail occurs in large quantities over the ultimate load accompanying sudden collapse of the structure. The failure appearance of model BE is shown in Fig. 14. In any cases, although matrix and fiber failure occur locally in accordance with the change of load, shear failure propagates to the longitudinal direction of the rod according to the increase of load accompanying a suddenly large deformation. It is thought that fiber failure disenables the rod to carry the additional load in tension specimens, and that a large

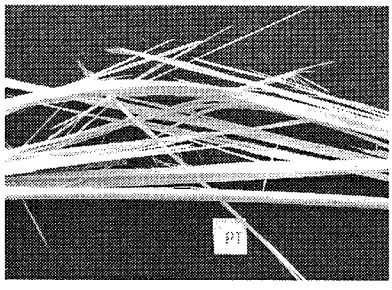

Fig. 11 Failure appearance of model TA.

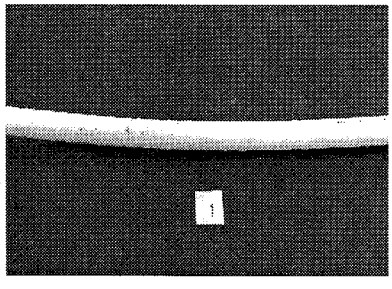

Fig. 12 Failure appearance of model TE.

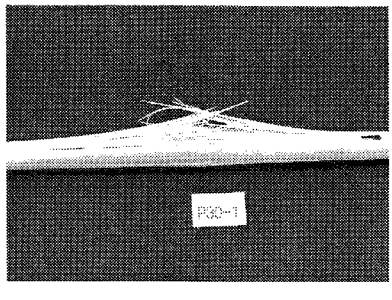

Fig. 13 Failure appearance of model BA.

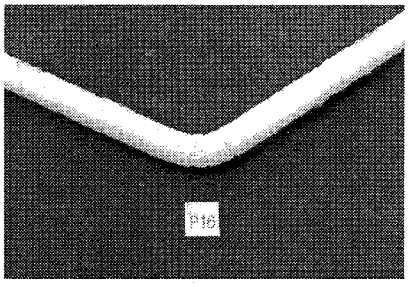

Fig. 14 Failure appearance of model TE.

deformation with crack to the longitudinal direction of the rod due to shear failure disenables the rod to carry the additional load after the ultimate load. Also, the tension fiber failure modes appear first in no-wound tension specimens, and the tension matrix fails first in wound tension specimens. It is thought that the 0° fiber carries the load mainly in no wound specimen and that the winding fiber influences the 0° fiber in load carrying.

6. Conclusion

In this study, buckling, postbuckling, and failure characteristics of the pultruded-wound hollow rod were analyzed using the finite element method based on the updated Lagrangian formulation. The progressive failure analysis approach is introduced in the finite element method. Experiments were performed to verify the finite element analysis of the pultruded-wound hollow rod. The agreement between the analysis and the experiment for buckling load, postbuckling ultimate load, and failure characteristics in both tension and bending were good. It was possible to depict the global of pultruded-wound hollow rod by modeling the rod as degenerated shell elements. Generally an increase of buckling load and postbuckling ultimate load can not be expected in wound tension specimen except for TW. This shows that reasonable winding causes the ultimate load to increase. In the case of bending behavior, BZ, BW and BX increased the buckling load and the postbuckling ultimate load.

However, global bending behavior of the specimen was not affected by a specific component of bending stiffness matrix but by coupling action of various stiffness matrix. The tension fiber failure results in failure of structure in tension specimen. The shear failure of the bending specimen causes the specimen to crack in the longitudinal direction over the entire area. Then, the specimen results in no additional load carrying following an exceeding deformation. The developed pultruded-wound process may be applied to manufacturing the Rebar which can be used as reinforcement to concrete.

References

1) Price H.L, "Curing and Flow of Thermosetting Resins for Composite Material Processing," Ph D thesis, Old Dominion University.
2) Sumerak J.E, "Understanding Pultrusion Process Variables for the First Time," *40th annual conference, Composite Institute SPI Inc*, Jan.28-Feb.1,1985, pp. 2-13.
3) Raper K.S,, Roux J.A,, Mccarty T.A,, Vaughan J.G. "Investigation of the pressure behavior in a pultrusion die for graphite/epoxy composites," *Composites; Part A*, 30, 1999, pp. 1123-1132.
4) Batch G.L., Macosko C.W, "Analysis of pressure, pulling force, and Sloughing in Pultrusion," *5th AIAA/ASME Thermophysics and Heat Transfer Conference*, June 1990.
5) Sharma D,, Mccarty T.A,, Roux J.A,, Vaughan J.G., "Investigation of dynamic pressure behavior in a pultrusion die," *Journal of Composite Material*, 1998, pp. 929-950.
6) Moschiar S.M,, Rebored M.M,, Kenny J.M,, Vazqez A., "Analysis of pultrusion Processing of Composites of Unsaturated Polyester Resin with Glass Fibers," *Polymer Composites*, June, 1996, 17, No. 3.
7) Kim Z.G., Hong C.S., Kim C.G.. "Postbuckling Analysis of Stringer-Stiffened Composite Laminated Cylindrical Panels," *Journal of Reinforced Plastics and Composites*, 14, Aug. 1995.
8) Bathe K.J,, "Finite element procedures in Engineering Analysis," 1985 London;prentice-Hall.